DYNAMIC ANALYSIS OF SWEPT-TIP BLADES THROUGH ADVANCED BEAM FORMULATIONS

Matteo Filippi
matteo.filippi@polito.it
PhD, Reseach Fellow
Dept. of Mechanical and Aerospace Eng.
Politecnico di Torino, Italy

Erasmo Carrera
erasmo.carrera@polito.it
Prof. of Aerospace Structures and Aeroelasticity
Dept. of Mechanical and Aerospace Eng.
Politecnico di Torino, Italy

ABSTRACT

The Carrera Unified Formulation (CUF) is here used to perform dynamic analyses of rotating structures. The hierarchical feature of CUF enables refined kinematic theories to be obtained in a systematic way. The displacement field components can be approximated using an arbitrary number of generic functions of the cross-sectional coordinates (x,z). In this work, both Taylor- and Lagrange-like polynomial expansions are used. The Finite Element technique along the longitudinal direction (y) of the structure is used to solve the weak form of the three-dimensional differential equations of motion in terms of $fundamental\ nuclei$, whose forms do not depend on the adopted kinematic assumptions. Structures that rotate about either transversal or longitudinal axis can be analysed by including gyroscopic and stiffening contributions. In particular, the dynamic characteristics of advanced rotary-wing configurations made of metallic, and composite materials are studied. Moreover, further simulations are performed on a three-layered blade with a viscoelastic core to evaluate the capabilities of 1D-CUF elements when structures with significant material anisotropy are considered. Current results are compared with theoretical and experimental solutions, when available. Comparisons reveal that the present one-dimensional formulation combines a relevant accuracy with a low computational cost.

1 INTRODUCTION

Over the years, the intrinsic 1D nature of rotors and the low computational cost have motivated the extensive use of the beam formulations in the study of the rotor dynamics. Many works have been devoted to the use of Euler-Bernoulli and Timoshenko theories for investigating the vibrational behavior of spinning shafts [1] and centrifugally stiffened beams [2]. However, the complexity of actual structures and the use of anisotropic materials have determined the need to improved the assumed kinematics with respect to the classical models. To this end, advanced 1D formulations encompassing the effects of transverse shear, cross-sectional warping and, non-uniform torsion have been proposed. The enhanced features of these models have been evaluated through stability and critical speed analyses performed on thin-walled box beams and cylinders made of composite materials [3]. Although the significant improvements deriving from the advanced 1D formulations, their use is restricted to rotors with compact cross-sections. When the deformability is no longer negligible, shell and solid solutions are required in order to include the centrifugal effects properly. Hence, thin and thick walled cylinders, discs as well as multi-section rotors are typically modeled through combinations of 1D, 2D and solid finite elements [4]. Nevertheless, this modeling technique may present two drawbacks: 1) high computational cost, especially when solid elements are being used in the model; 2) the assemblage of different finite elements types. In order to overcome these issues, reduction techniques [5] and rigid/transition elements [6] can be adopted.

This paper proposes advanced classes of beam finite elements for structural analyses of rotors. The present methodology exploits the one-dimensional Carrera Unified Formulation (1D-CUF), which enables one to go beyond the classical kinematic assumptions. CUF is a mathematical tool, which makes it possible to derive, at least theoretically, any kind of sophisticated displacement models. The 1D-CUF elements have been extensively adopted for the study of the mechanical response of complex-shaped structures made of isotropic and composite materials according to either equivalent single layer (ESL) or layer-wise (LW) approach. Within the ESL context, arbitrary N-order power series expansions (referred as to 'TEN') of the cross-sectional coordinates were used to approximated the tree components of the displacement fields ($\boldsymbol{u}^T$=[u_x, u_y, u_z]). The 'TEN' models provided encouraging results for shafts made of isotropic [7] and orthotropic materials [8], for thin/thick rotating shells [9] and, for straight rotary-wing configurations [10]. These results demonstrated that TE

models are efficient for prismatic structures, but they can show limitations when the components of the rotor present different deformability. In order to overcome this shortcoming, the LW approach has been recently adopted. The LW 1D-CUF elements have been derived by exploiting the inherent capabilities of Lagrange-type expansions (referred as to 'LE'), which make possible local refinements, depending on the characteristics of the rotor component (deformability, mechanical properties, etc.). To evaluate the enhanced features of 'LE' elements, vibrational analyses have been performed on metallic rotors (rings, discs, and bladed shafts) [11], and on layered viscoelastic structures [12].
The proposed unified formulation enables one to derive the equations of motion in a fully three-dimensional form by including all effects due to the rotational speed namely the Coriolis term, the spin softening and the centrifugal stiffening. In this work, close attention is given to the dynamical response of real rotary-wing configurations. In particular, the effects of the sweep angle and the use of viscoelastic materials on the natural frequencies are being evaluated. Owing to their computational efficiency and accuracy, the 1D-CUF elements enable one to consider many structural configurations. This capability can significantly facilitate the design process by providing useful insights on the dynamic response of the rotary wings.

2 KINETIC AND POTENTIAL ENERGIES

To obtain the equations of motion of a structure that is rotating with a constant speed Ω, Hamilton's Principle is used

$$\delta \int_{t_0}^{t_1} (T - U_{tot})\, \mathrm{d}t = 0 \tag{1}$$

where T and U are the kinetic and the potential energies in the co-rotating reference frame, and δ is the virtual variation of the functional (see [7]). The absolute velocity of a point P at a distance $\boldsymbol{r}_{tot}$ from the neutral axis is the sum of the relative velocity and the transfer velocity

$$v_{abs} = v_{rel} + v_t = \dot{\boldsymbol{u}} + \boldsymbol{\Omega} \times \boldsymbol{r}_{tot} \tag{2}$$

$$\boldsymbol{\Omega} = \begin{bmatrix} 0 & -\Omega_z & \Omega_y \\ \Omega_z & 0 & 0 \\ -\Omega_y & 0 & 0 \end{bmatrix}$$

According to Eq.2, it is possible to derive the kinetic energy, whose explicit expression can be found in [9].

In the linearized analysis, the total potential energy, U_{tot}, is given by the sum of the elastic term U and the geometric contribution U_{σ_0}, which is due to the pre-stress σ_0 (or pre-strain ϵ_0) field generated by centrifugal or thermal effects. The expressions of U is

$$U = \frac{1}{2} \int_V \boldsymbol{u}^T \boldsymbol{D}^T \boldsymbol{C} \boldsymbol{D} \boldsymbol{u}\, \mathrm{d}V$$

The linear strain-displacement relation is defined by the differential operator $\boldsymbol{D}$ [13], while the expressions of the stiffness coefficients of $\boldsymbol{C}$ matrix for orthotropic and viscoelastic materials can be found in [14] and [12], respectively.
The expression of the geometric term is

$$U_{\sigma_0} = \int_V \boldsymbol{\sigma}_0^{\mathrm{T}} \boldsymbol{\epsilon}^{nl}\, \mathrm{d}V$$

where $\boldsymbol{\epsilon}^{nl}$ are the non-linear components of the strain field. For example, the expression of σ_0 for a centrifugally stiffened blade (Ω_y=0) is

$$\sigma_0 = \Omega_z^2 \rho [r_h L - r_h y + 0.5(L^2 - y^2)]$$

where L, and r_h are the length of the beam, and the dimension of the hub, respectively.

3 CARRERA UNIFIED FORMULATION

Within the CUF framework, the displacement field is an expansion of generic cross-sectional functions, F_τ

$$\mathbf{u}(x,y,z) = F_\tau(x,z)\mathbf{u}_\tau(y) \qquad \tau = 1,2,\ldots,M \tag{3}$$

where $\mathbf{u}_\tau$ is the vector of the *generalized* displacements, M is the number of terms of the expansion and, in accordance with the generalized Einstein's notation, τ indicates summation. In this work, two kinds of expansions are considered, namely the Taylor-like and the Lagrange-like expansions. As far as the TE polynomials are concerned, the displacement field up to the first order (TE1) is

$$\begin{gathered} u(x,y,z) = u_1(y) + x\ u_2(y) + z\ u_3(y) \\ v(x,y,z) = v_1(y) + x\ v_2(y) + z\ v_3(y) \\ w(x,y,z) = w_1(y) + x\ w_2(y) + z\ w_3(y) \end{gathered}$$

while, for the nine-point Lagrange element (LE9), the interpolation functions become

$$F_\tau = \tfrac{1}{4}(r^2 + r\ r_\tau)(s^2 + s\ s_\tau) \qquad \tau = 1,3,5,7$$

$$F_\tau = \tfrac{1}{2}s_\tau^2(s^2 - s\ s_\tau)(1 - r^2) + \tfrac{1}{2}r_\tau^2(r^2 - r\ r_\tau)(1 - s^2) \qquad \tau = 2,4,6,8$$

$$F_\tau = (1 - r^2)(1 - s^2) \qquad \tau = 9$$

where r and s vary from -1 to $+1$. r_τ and s_τ are the coordinates of the nine points expressed in the natural coordinate frame (see [11]).
The generalized displacement vector along the beam axis is interpolated through a classical finite element technique

(4) $$\mathbf{u}_\tau(y,t) = N_i(y)\mathbf{q}_{\tau i}(t)$$

where $\mathbf{q}_{\tau i}^T(t) = [q_{u_{x_{\tau i}}}, q_{u_{y_{\tau i}}}, q_{u_{z_{\tau i}}}]$ is the nodal displacement vector, and N_i are the lagrangian shape functions along the longitudinal axis (see [13] (§5.2.2)).

4 GOVERNING EQUATIONS

The equations of motion are derived by Eq.1, in which the kinetic and potential energies are expressed using the CUF approximations (Eqs.3, and 4). The homogeneous equations of motion in CUF form are

(5) $$\boldsymbol{M}^{\tau sij}\ddot{\boldsymbol{q}} + \boldsymbol{G}_\Omega^{\tau sij}\dot{\boldsymbol{q}} + (\boldsymbol{K}^{\tau sij} + \boldsymbol{K}_\Omega^{\tau sij} + \boldsymbol{K}_{\sigma 0}^{\tau sij})\boldsymbol{q} = 0$$

where $\boldsymbol{M}^{\tau sij}$ is the mass matrix, $\boldsymbol{G}_\Omega^{\tau sij}$ is the Coriolis term, $\boldsymbol{K}_\Omega^{\tau sij}$ is the softening matrix, $\boldsymbol{K}_{\sigma 0}^{\tau sij}$ is the centrifugal contribution, and $\boldsymbol{K}^{\tau sij}$ is the stiffness matrix. Neither the nature of functions F_τ nor their number N modifies the expressions of these mathematical operators, which are traditionally called *fundamental nuclei*. The explicit expressions of the *fundamental nuclei* can be found in [15]. The complete structural matrices related to the adopted mathematical model are being obtained through the assembly technique schematically shown in Fig.1.

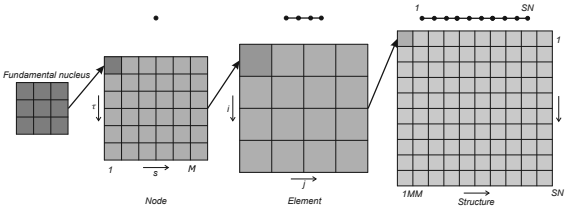

Figure 1: Graphical representation of the assembly procedure.

The numbers of degrees of freedom (DOFs) required for the CUF models have been obtained using the following formula

$$DOFs = (3 \times M) \times SN$$

where 'SN' stands for the structural beam nodes along the longitudinal axis.
The homogeneous equations are solved assuming a periodic solution $\mathbf{q} = \bar{\mathbf{q}}e^{i\omega t}$ in order to obtain natural frequencies and normal modes of the rotor.

(6) $$\bar{\mathbf{q}}e^{i\omega t}\left[(\boldsymbol{K} + \boldsymbol{K}_{\sigma_0} - \mathbf{K}_\Omega) + (\boldsymbol{G}_\Omega)i\omega - (\boldsymbol{M})\omega^2\right] = 0$$

The quadratic eigenvalue problem of Eq.(6) is solved as previously done in [7] and [8].

5 NUMERICAL RESULTS

Although the proposed formulation enables rotary-wing and spinning structures to be considered, the following section aims of presenting analyses performed on straight and swept-tip blades made of isotropic, composite and viscoelastic materials.

5.1 Isotropic blades

A metallic blade, which is schematically shown in Fig.2, has been considered. The Young's modulus is E=73.08 [GPa], Poisson's ratio is ν=0.325, and the density is ρ=2682 [kg m^{-3}].

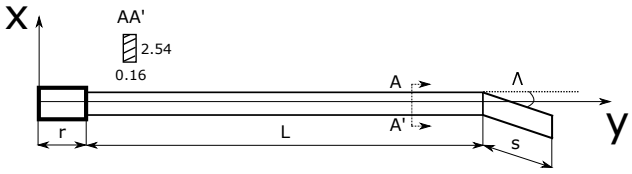

Figure 2: Swept-tip blade configuration.

Firstly, for L=80.01, s=15.24, r=6.35, and different values of Λ, Tabs. 1-4 list the natural frequencies of structures computed with the first-order shear deformation theory (FSDT) and two higher-order 1D models (TE2-TE3) using a mesh with 11 4-node elements along the y-axis. The notations "B" and "T" indicate vibration modes dominated by bending and torsional deformation, respectively. Current results have been compared with solutions reported in [16], where a non-linear beam formulation was validated against theoretical and experimental data presented in [17]. Due to the significant twist-bending coupling, the first-order shear deformation theory provided inaccurate results for swept-tip configurations. Conversely, comparisons have revealed good correlations between the TE predictions and reference solutions for all combinations of sweep angle and rotational speed. In the second application, according to Fig.2, dimensions L, s, and r have been assumed equal to 16.5, 15.24 and 69.85 [cm]. The Young's modulus is E=68.9 [GPa], Poisson's ratio is ν=0.3, and the density is ρ=2700 [kg m^{-3}]. Natural frequencies are shown in Figs.3 and 4 as functions of the rotational speed for Λ=0^o and 45^o, respectively. For both cases, TE3 results have been reported together with the solutions provided in [18], where the results obtained with a solid-shell fi-

nite element were compared with those derived from a non-linear 1D formulation [19].

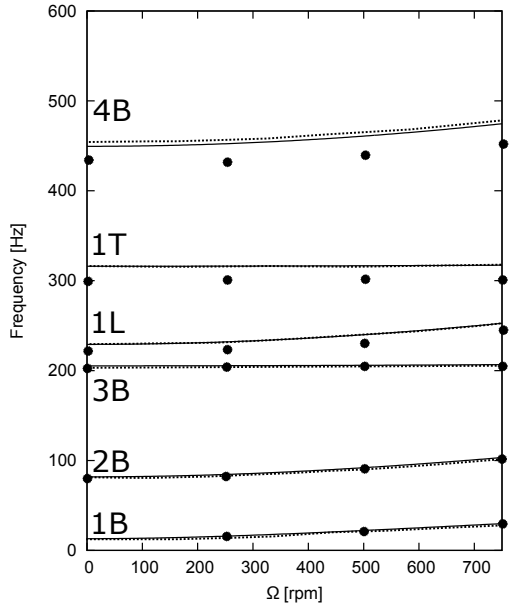

Figure 3: Λ=0^o, L = 16.5, s = 15.24 and r = 69.85 [cm]. '–': TE3, '- - -': [18], '•': [19]

For Λ=0^o, it is observed that TE3 results strongly agree with those predicted by the solid-shell solution while slight discrepancies exist with the 1D approach. As far as the second configuration is concerned, the frequencies related to the first four modes basically match those presented in [18]. Conversely, for the coupled modes 4B/1T and 5B/1T, the three approaches predicted different results. The maximum discrepancy between the 1D CUF and the solid-shell solution is about 10%.

5.2 Composite blades

To evaluate the capabilities of the presented methodology in the study of swept-tip blades made of composite material, a structure with a chord and a thickness equal to 1.79578 and 0.30734 [cm], respectively, has been considered. The other geometric dimensions are L=80.01, s=15.24, r=6.35, and Λ=45^o (see Fig.2), while the material properties are E_{11}=142, E_{22} = E_{33} = 9.78 [GPa], ν_{12}=ν_{13}=0.42, ν_{32}=0.54, G_{12}=G_{13}=6.14, G_{32}=5.52 [GPa], and ρ= 1538 [kg m^{-3}].
The analyses have been performed using the TE3 and TE4 theories for two different lamination schemes: θ =0^o and θ =15^o. The related results are shown in Figs. 5 and 6. Also for these cases, the solutions presented in [16] have been reported as reference values. For θ =0^o (Fig. 5), the 1D results agree well with the experimental and theoretical data, except for slight discrepancies in the com-

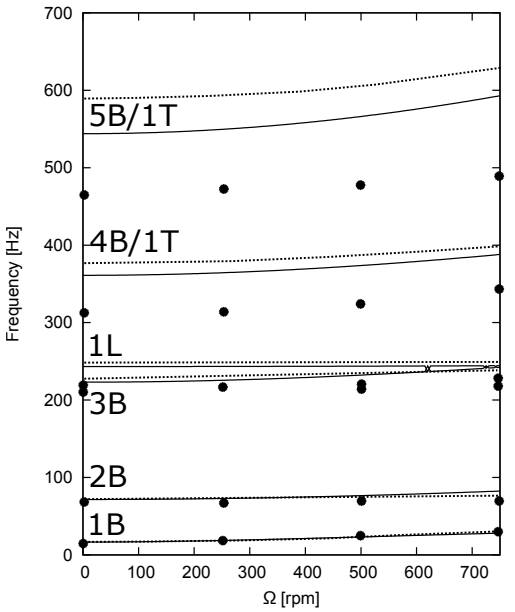

Figure 4: Λ=45^o, L = 16.5, s = 15.24 and r = 69.85 [cm]. '–': TE3, '- - -': [18], '•': [19]

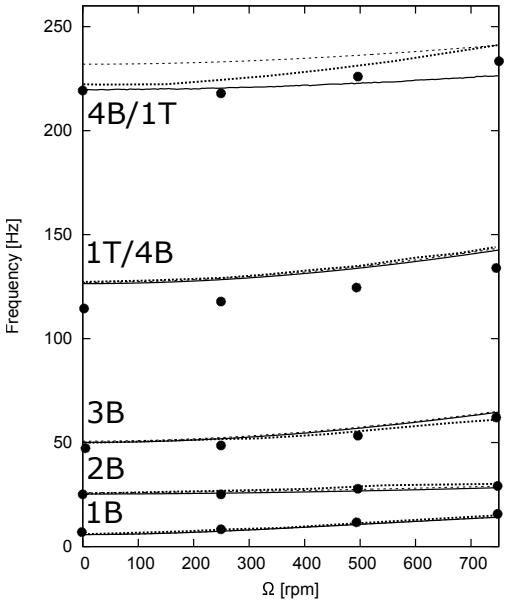

Figure 5: Composite blade [0^o]. '–': TE4, '- - -': TE3, '- - -': Theory [16], '•': Exp. [17]

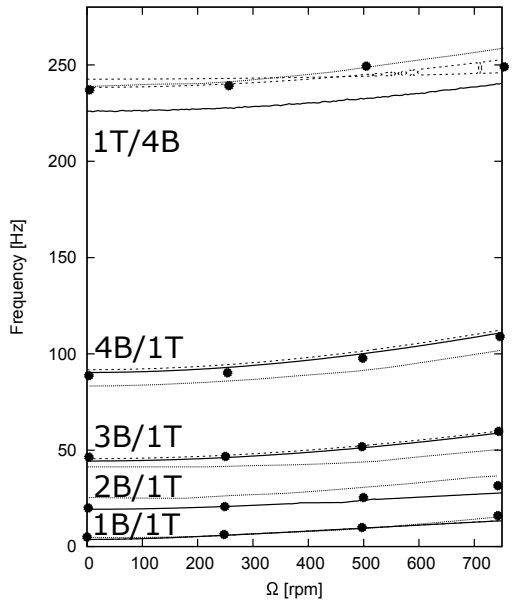

Figure 6: Composite blade [15^o]. '–': TE4, '- - -': TE3, '- - -': Theory [16], '•': Exp. [17]

putation of the 4B/1T frequency. As far as the second lamination scheme (Fig. 6) is concerned, it can be observed a good correlation between the experimental data and the current solutions for the first four frequencies. Conversely, the reference theoretical approach provided lower values of natural frequencies.

5.3 Layered viscoelastic blades

A symmetric sandwich beam has been considered. The structure consisted of a viscoelastic core with thickness h_c = 0.127 [mm] constrained between two metallic layers with Youngs modulus E_f = 69 [GPa], density ρ_f = 2766 [kg m3], Poissons ratio ν_f = 0.3 and thickness h_{fb} = h_{ft} = 1.524 [mm]. The beam length and the width have been assumed equal to L=177.8 [mm] and b=12.7 [mm], respectively. This beam configuration was extensively analysed in previous works by assuming either constant or frequency-dependent properties of the core. For the case of constant values of η_c, the storage core modulus, the density and the Poissons ratio of the core have been assumed equal to E_{c0} = 1.794 [MPa], ρ_c = 968.13 [kg m3] and ν_c = 0.3, respectively. Table 5 list the damped frequencies and the corresponding modal loss factors for $\eta_c = 1.5$. The results obtained with 3LE9 and 8 4 node-beam elements are compared with solutions available in the literature and those derived from a convergent 3D finite element model. The current values compare well with both reference solutions in terms of both damped frequencies and modal loss factors. Also, it should be observed that the present layer-wise approach predicted accurate results for torsional deformations. For the same value of η_c, Fig. 7 shows the first two flexural and the first torsional damped frequencies with corresponding modal loss factors as functions of the rotational speed.

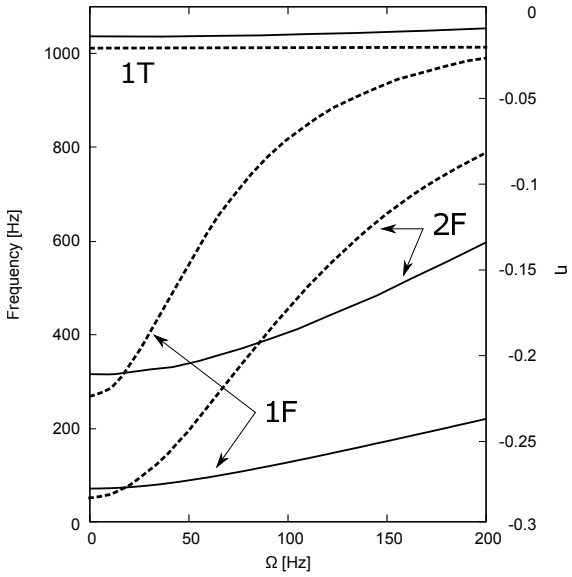

Figure 7: Damped frequencies, '–', and modal loss factors, '- - -', of viscoelastic blade. η_c=1.5.

It should be observed that the absolute values of frequencies and loss factors exhibit different variations when the velocity increases. The centrifugal effects tend to increase the blade bending stiffness, therefore reducing the effectiveness of the damping layer. For the torsional, any significant variations have been observed within the considered speed range. Figures 8 and 9 show the variations of damped frequencies and modal loss factors of the first two bending modes as functions of η_c.
The analyses have been performed at three different velocities $\Omega = 0$, 100 and 200 [Hz]. The simulations reveal that the modal loss factor related to the first flap mode is higher than η_2 for values of η_c lower than 0.8. The material loss factor represents, therefore, an effective design parameter for the controlling of vibrations and dynamic instabilities. The proper value of such quantity could be determined through optimization processes, which require the use of reliable and computationally effective mathematical tools. Hence, the 1D-CUF approach may represent a valuable methodology for this kind of analysis.

6 CONCLUSION

In this paper, advanced beam formulations were used for the study of the dynamic response of structures that can rotate about the longitudinal or transversal axis. The three-dimensional equations of motion, which were derived from Hamilton's Principle, were

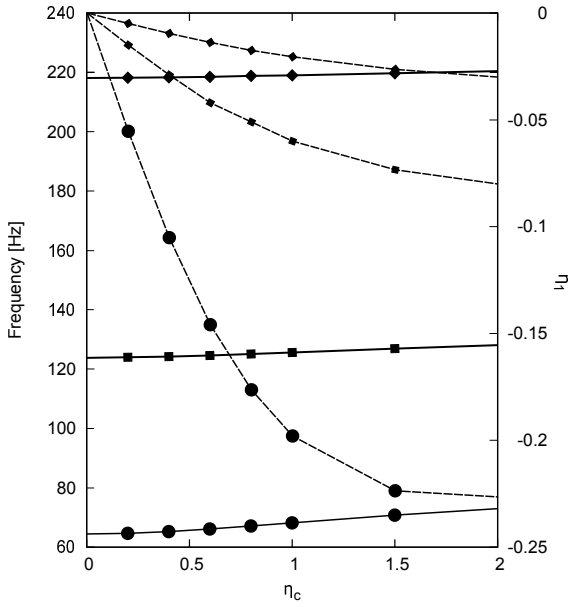

Figure 8: Damped frequencies, '–', and modal loss factors, '- - -', of the first flap mode. •: $\Omega = 0$, □: $\Omega = 100$, and ⋄: $\Omega = 200$ [Hz].

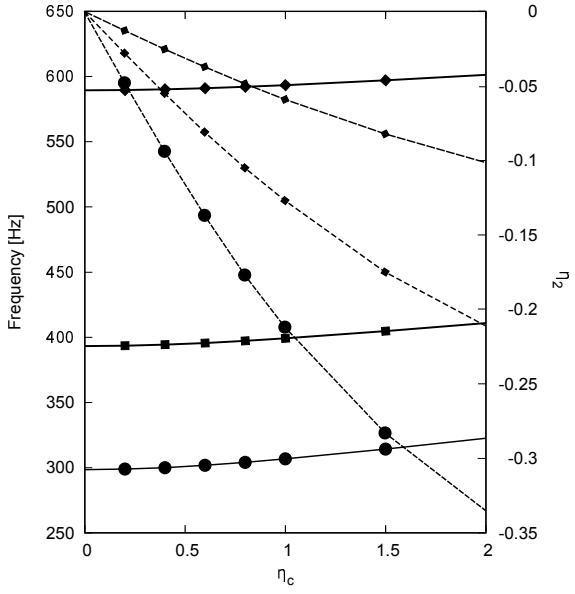

Figure 9: Damped frequencies, '–', and modal loss factors, '- - -', of the second flap mode. •: $\Omega = 0$, □: $\Omega = 100$, and ⋄: $\Omega = 200$ [Hz].

obtained in the CUF framework. All mathematical operators, namely the mass matrix, the stiffness matrix, the Coriolis matrix and the centrifugal matrices were written in terms of fundamental nuclei, whose expressions do not depend on adopted kinematic theories. Close attention was given to swept-tip blade configurations made of isotropic and orthotropic materials. Moreover, a laminated straight beam with a viscoelastic core was analysed in order to show the capabilities of 1D-CUF elements when structures with significant mechanical anisotropy are considered. Current solutions were compared with theoretical and experimental results published in the literature. These comparisons revealed that the 1D-CUF approach provides accurate results for all considered structural problems. The refined beam models are able to detect coupling effects due to the geometry and the lamination scheme.

References

[1] C.W. Bert and C.D. Kim. Whirling of composite-material driveshafts including bending-twisting coupling and transverse shear deformation. *Journal of Vibration and Acoustics*, 17:17–21, 1995.

[2] SC Lin and KM Hsiao. Vibration analysis of a rotating timoshenko beam. *Journal of Sound and Vibration*, 240(2):303–322, 2001.

[3] L. Librescu, S.Y. Oh, and O. Song. Spinning thin-walled beams made of functionally graded materials: modeling, vibration and instability. *European Journal of Mechanics A/Solids*, 23:499–515, 2004.

[4] G.H. Jang and J.H. Han. Finite element modal analysis of a spinning flexible disk-spindle systemin a hdd considering the flexibility of complicated supporting structure. *Microsystem Technologies*, 11:766–778, 2005. DOI10.1007/s00542-005-0579-4.

[5] Matthew B Wagner, Amir Younan, Paul Allaire, and Randy Cogill. Model reduction methods for rotor dynamic analysis: a survey and review. *International Journal of Rotating Machinery*, 2010, 2011.

[6] G. Genta, Chen Feng, and A. Tonoli. Dynamics behavior of rotating bladed discs: A finite element formulation for the study of second and higher order harmonics. *Journal of Sound and Vibration*, 329:5289–5306, 2010.

[7] E. Carrera, M. Filippi, and E. Zappino. Analysis of rotor dynamic by one-dimensional variable kinematic theories. *Journal of Engineering for Gas Turbines and Power*, 135:092501, 2013. DOI: 10.1115/1.4024381.

[8] E. Carrera and M. Filippi. Variable kinematic one-dimensional finite elements for the analysis of rotors made of composite materials. *Journal of Engineering for Gas Turbines and Power*, 136:092501, 2014. DOI: 10.1115/1.4027192.

[9] E. Carrera and M. Filippi. Vibration analysis of thin/thick, composites/metallic spinning cylindrical shells by refined beam models. *Journal of Vibration and Acoustics*, 137:031020, 2015. DOI: 10.1115/1.4029688.

[10] M Filippi and E Carrera. Flutter analysis of fixed and rotary wings through a one-dimensional unified formulation. *Composite Structures*, 133:381–389, 2015.

[11] E Carrera and M Filippi. A refined one-dimensional rotordynamics model with three-dimensional capabilities. *Journal of Sound and Vibration*, 366:343–356, 2016.

[12] Matteo Filippi, Erasmo Carrera, and Andrea M Regalli. Layer-wise analyses of compact and thin-walled beams made of viscoelastic materials. *Journal of Vibration and Acoustics*, 2016.

[13] E. Carrera, G. Giunta, and M. Petrolo. *Beam Structures. Classical and Advanced Theories.* Wiley, 2011.

[14] Erasmo Carrera and Matteo Filippi. Variable kinematic one-dimensional finite elements for the analysis of rotors made of composite materials. *Journal of Engineering for Gas Turbines and Power*, 136(9):092501, 2014.

[15] Matteo Filippi, Erasmo Carrera, et al. Capabilities of 1d cuf-based models to analyze metallic/composite rotors. In *8th Australasian Congress on Applied Mechanics: ACAM 8*, page 315. Engineers Australia, 2014.

[16] Dewey H Hodges, Xiaoyang Shang, and Carlos ES Cesnik. Finite element solution of nonlinear intrinsic equations for curved composite beams. *Journal of the American helicopter society*, 41(4):313–321, 1996.

[17] Jeanette J Epps and Ramesh Chandra. The natural frequencies of rotating composite beams with tip sweep. *Journal of the American Helicopter Society*, 41(1):29–36, 1996.

[18] Young-Jung Kee and Sang-Joon Shin. Structural dynamic modeling for rotating blades using three dimensional finite elements. *Journal of Mechanical Science and Technology*, 29(4):1607–1618, 2015.

[19] Hao Kang, Chongseok Chang, Hossein Saberi, and Robert A Ormiston. Assessment of beam and shell elements for modeling rotorcraft blades. *Journal of Aircraft*, 51(2):520–531, 2014.

[20] M Bilasse, EM Daya, and L Azrar. Linear and nonlinear vibrations analysis of viscoelastic sandwich beams. *Journal of Sound and vibration*, 329(23):4950–4969, 2010.

Speed [rpm]	Mode	FSDT	TE2	TE3	Theory [17]	Exp. [17]	Theory [16]
0	1B	1.487	1.502	1.496	1.41	1.41	1.41
	2B	9.320	9.415	9.375	9.24	9.24	9.99
	3B	26.09	26.39	26.25	24.8	26.2	26.2
	4B/1T	51.14	51.83	51.46	49.1	51.5	51.5
	5B/1T	84.54	85.91	85.10	82.4	84.8	87.9
	1T/5B	-	106.4	106.4	104.	99.5	102.
500	1B	9.191	9.217	9.210	9.24	9.24	10.1
	2B	23.83	23.91	23.89	23.9	23.9	25.0
	3B	44.55	44.78	44.69	44.0	44.0	45.5
	4B/1T	72.60	73.15	72.89	-	-	-
	5B/1T	108.0	109.2	108.6	-	-	-
	1T/5B	-	106.8	106.8	-	-	-
750	1B	13.55	13.58	13.57	13.6	13.6	14.7
	2B	34.00	34.09	34.07	34.0	34.0	36.1
	3B	59.48	59.71	59.64	59.6	59.6	62.2
	4B/1T	91.80	92.30	92.10	90.2	92.4	92.4
	5B/1T	130.8	131.8	131.3	131.	131.	135.
	1T/5B	-	107.3	107.3	104.	104.	104.

Table 1: Natural frequencies of metallic blade (see Fig.2). Λ=0^o, L = 80.01, s = 15.24 and r = 6.35 [cm].

Damped Frequencies [Hz]								
	f_1	f_2	f_3	f_4	f_5	f_6	f_7^+	f_8^+
Ref. [20]	69.9	309.1	755.2	1401.4	2268.4	3352.3	-	-
3D FE^c	70.645	313.575	762.520	1409.877	2279.704	3367.621	1003.142	3036.941
LE9	70.643	313.614	762.687	1410.441	2281.621	3373.871	1032.369	3124.899
Absolute values of Modal Loss Factors $\times$ 100								
Ref. [20]	22.95	29.55	21.75	13.05	8.4	5.7	-	-
3D FE^c	22.626	28.908	21.514	12.923	8.398	5.727	2.146	2.185
LE9	22.333	28.319	21.272	12.877	8.390	5.726	2.068	2.119

'+': torsional mode shapes.

Table 5: Frequencies and modal loss factors for $\eta_c = 1.5$

Speed [rpm]	Mode	FSDT	TE2	TE3	Theory [17]	Exp. [17]	Theory [16]
0	1B	1.503	1.518	1.512	1.62	1.93	1.62
	2B	9.422	9.483	9.443	9.33	9.89	9.33
	3B	26.38	26.16	26.02	25.4	26.4	26.4
	4B/1T	51.70	50.00	49.65	48.3	50.3	50.3
	5B/1T	85.47	80.18	79.53	77.2	81.3	81.3
	1T/5B	127.7	110.1	109.6	109.	105.	113.
500	1B	9.198	9.186	9.180	9.26	10.1	9.26
	2B	23.88	23.24	23.22	23.5	25.1	23.5
	3B	44.73	42.64	42.56	43.4	43.4	41.7
	4B/1T	73.02	68.51	68.28	-	-	-
	5B/1T	108.8	99.69	99.29	-	-	-
	1T/5B	152.4	125.7	125.3	-	-	-
750	1B	13.55	13.47	13.46	13.6	14.4	13.6
	2B	34.04	31.90	31.88	33.6	34.8	33.1
	3B	59.64	54.64	54.56	57.1	54.6	53.4
	4B/1T	92.17	84.62	84.45	87.5	85.3	82.8
	5B/1T	131.4	118.0	117.8	115.	120.	120.
	1T/5B	177.8	142.2	141.7	137.	144.	144.

Table 2: Natural frequencies of metallic blade (see Fig.2). Λ=15^o, L = 80.01, s = 15.24 and r = 6.35 [cm].

Speed [rpm]	Mode	FSDT	TE2	TE3	Theory [17]	Exp. [17]	Theory [16]
0	1B	1.553	1.568	1.568	1.57	1.76	1.57
	2B	9.733	9.706	9.663	9.49	10.1	9.49
	3B	27.25	25.56	25.41	24.1	25.3	24.1
	4B/1T	53.40	45.87	45.53	45.3	46.7	45.3
	5B/1T	88.28	74.54	73.90	72.5	76.3	76.3
	1T/5B	131.9	114.0	112.9	111.	116.	121.
500	1B	9.221	9.123	9.116	9.28	10.2	9.28
	2B	24.03	21.70	21.66	22.9	23.7	22.6
	3B	45.29	38.69	38.57	40.7	38.1	36.4
	4B/1T	74.29	63.35	63.11	-	-	-
	5B/1T	111.0	97.05	96.57	-	-	-
	1T/5B	153.1	138.9	138.0	-	-	-
750	1B	13.58	13.21	13.20	13.7	14.9	13.7
	2B	34.16	27.55	27.48	32.5	31.1	30.0
	3B	60.11	49.02	48.91	54.9	47.1	45.4
	4B/1T	93.25	80.36	80.16	84.3	80.9	77.9
	5B/1T	133.4	119.3	119.0	118.	120.	118.
	1T/5B	181.0	163.5	162.9	159.	165.	173.

Table 3: Natural frequencies of metallic blade (see Fig.2). Λ=30^o, L = 80.01, s = 15.24 and r = 6.35 [cm].

Speed [rpm]	Mode	FSDT	TE2	TE3	Theory [17]	Exp. [17]	Theory [16]
0	1B	1.637	1.653	1.646	1.65	1.65	1.65
	2B	10.26	10.14	10.09	9.73	10.2	9.73
	3B	28.72	25.02	24.82	22.7	23.6	22.7
	4B/1T	56.29	42.57	42.19	40.3	42.4	40.3
	5B/1T	93.06	72.61	71.94	69.6	72.0	75.4
	1T/5B	139.1	115.7	114.4	114.	112.	125.
500	1B	9.258	9.103	9.092	9.34	10.4	9.34
	2B	24.28	20.49	20.40	21.9	21.9	21.9
	3B	46.27	35.88	35.70	38.8	33.7	32.4
	4B/1T	76.47	60.43	60.17	-	-	-
	5B/1T	115.0	95.33	94.80	-	-	-
	1T/5B	162.1	140.5	139.4	-	-	-
750	1B	13.62	13.03	13.01	13.7	15.0	13.9
	2B	34.38	24.63	24.49	28.8	26.5	26.5
	3B	60.93	46.05	45.90	49.5	43.2	41.4
	4B/1T	95.13	77.58	77.35	81.6	76.5	73.9
	5B/1T	136.8	117.3	116.9	121.	116.	116.
	1T/5B	186.5	165.8	164.9	165.	161.	172.

Table 4: Natural frequencies of metallic blade (see Fig.2). Λ=30^o, L = 80.01, s = 15.24 and r = 6.35 [cm].